Effective simulation for robust inverse lithography using convolution-variation separation method

Wen Lv [a], Shiyuan Liu [a, b, *], Xinjiang Zhou [a], and Haiqing Wei [a]

[a] State Key Laboratory of Digital Manufacturing Equipment and Technology, Huazhong University of Science and Technology, Wuhan 430074, China

[b] Wuhan National Laboratory for Optoelectronics, Huazhong University of Science and Technology, Wuhan 430074, China

ABSTRACT

As critical dimension shrinks, pattern density of integrated circuits gets much denser and lithographic process variations become more pronounced. In order to synthesize masks that are robust to process variations, the average wafer performance with respect to process fluctuations is optimized. This approach takes into account process variations explicitly. However, it needs to calculate a large number of optical images under different process variations during its optimizing process and thus significantly increases the computational burden. Most recently, we proposed a convolution-variation separation (CVS) method for modeling of optical lithography, which separates process variables from the coordinate system and hence enables fast computation of optical images through a wide range of process variations. In this work, we detail the formulation of robust inverse lithography making use of the CVS method, and further investigate the impacts of arbitrary statistical distribution of process variations on the synthesized mask patterns.

Keywords: optical lithography, robust inverse lithography, process variations, distribution of process variations, convolution-variation separation (CVS) method.

1. INTRODUCTION

Inverse lithography technology (ILT) is considered as an effective and economically viable way to meet various challenges in current and future technology nodes [1, 2]. Its objective is to synthesize an input mask to deliver a desired output pattern on the wafer. Currently, as critical dimension (CD) shrinks, pattern density of integrated circuits gets much denser and lithographic process variations, such as lens-wafer defocus and exposure dose variation, become more pronounced. It therefore requires through process window compensated approaches to synthesize masks for the high volume production. To this end, the average wafer performance with respect to process fluctuations is optimized via minimizing the expectation of the difference between the output pattern and the desired pattern [3, 4]. This approach takes into account process variations explicitly, and is well understood and easily accomplished. It is a commonly used robust ILT, and one of its drawbacks is that it needs to calculate a large number of optical images under different process variations during its optimizing process.

The imaging formation in optical lithography, especially adopted in ILT, is usually formulated in a bilinear form [5] according to Hopkins' imaging theory [6], in which the transmission cross coefficient (TCC) matrix is introduced as a combination of the illumination source and pupil, and the optical image can be calculated by an equation with a four-fold integral. In order to simplify the integral operation, the concept of sum of coherent systems [7-9], which approximates the partially coherent system by the superposition of coherent systems, was introduced and it achieved a significant speedup by eigenanalyzing the TCC matrix and neglecting small eigenvalues. Nevertheless, the TCC kernels are usually obtained under the nominal (best) process condition, and an imaging simulator may have to repeat the costly TCC decomposition and mask-kernel convolutions when process parameters vary.

Most recently, we proposed a convolution-variation separation (CVS) method for modeling of optical lithography [10], which separates process variables from the coordinate system and hence enables fast computation of optical images

* Corresponding author: shyliu@mail.hust.edu.cn; phone: +86 27 87559543; webpage: http://www2.hust.edu.cn/nom.

Optical Microlithography XXVII, edited by Kafai Lai, Andreas Erdmann, Proc. of SPIE Vol. 9052, 90522C © 2014 SPIE · CCC code: 0277-786X/14/$18 · doi: 10.1117/12.2046322

Downloaded From: http://nanolithography.spiedigitallibrary.org/ on 04/11/2014 Terms of Use: http://spiedl.org/terms

through a wide range of process variations. The fundamental rationale behind the CVS method is that a physical quantity being dependent on both a spatial coordinate and other parameters can be represented by a sum of multiple series expansion terms, with each term consisting of one function dependent only upon the spatial coordinate and another function dependent only upon the other parameters. In this work, we provide detailed formulation of robust inverse lithography making use of the CVS method. In addition, we investigate the impacts of the statistical process variations distribution on the synthesized mask patterns in robust inverse lithography.

2. METHODLOGY

2.1 The lithography imaging model with process variations

In this work, we consider two main process variations in optical lithography, i.e., lens-wafer defocus and exposure dose variation. So the lithography imaging model is decomposed into two parts, namely the defocused optical image formation and the resist development with an exposure dose variation.

The defocused optical image $I(\mathbf{r}; h)$ generated by a partially coherent imaging system can be expressed by a bilinear transform in the spatial domain

$$I(\mathbf{r};h) = \iint D(\mathbf{r}-\mathbf{r}_1, \mathbf{r}-\mathbf{r}_2;\, h)\, M(\mathbf{r}_1) M^{\dagger}(\mathbf{r}_2) \mathrm{d}\mathbf{r}_1 \mathrm{d}\mathbf{r}_2, \tag{1}$$

where $\mathbf{r}$ is the two-dimensional (2D) spatial coordinate (x, y), h is the defocus, $M(\mathbf{r})$ is the mask transmittance function, † denotes complex conjugation, and

$$D(\mathbf{r}_1, \mathbf{r}_2; h) = J(\mathbf{r}_1 - \mathbf{r}_2) H(\mathbf{r}_1; h) H^{\dagger}(\mathbf{r}_2; h) \tag{2}$$

is called double-impulse response (DIR) function [5] whose Fourier transform is the familiar TCC [6]. Here, $J(\mathbf{r}_1, \mathbf{r}_2)$ is the mutual intensity function of the illumination source, and $H(\mathbf{r}; h)$ is the defocused point spread function (PSF) [4] of the optical system as

$$H(\mathbf{r};h) = \mathtt{IFT}\left\{ \tilde{H}(\mathbf{f}) \cdot \exp\left[j\pi h \frac{\mathrm{NA}^2}{\lambda} \mathbf{f}^2 \right] \right\}, \tag{3}$$

where $\mathbf{f}$ is the normalized pupil plane coordinate, $j = \sqrt{-1}$, NA is the numerical aperture, λ is the incident light wavelength, $\tilde{H}(\mathbf{f}) = \mathrm{circ}(|\mathbf{f}|)$ is the pupil function at the best focus without any aberrations, and $\mathrm{IFT}\{\cdot\}$ is the inverse Fourier transform. Intentionally, we expand the exponential function portion in Eq. (3) into Taylor series with the truncation order N as

$$\exp\left[j\pi h \frac{\mathrm{NA}^2}{\lambda} \mathbf{f}^2 \right] = \sum_{n=0}^{N} \frac{1}{n!} \left[j\pi h \frac{\mathrm{NA}^2}{\lambda} \mathbf{f}^2 \right]^n = \sum_{n=0}^{N} \frac{h^n}{n!} \left[j\pi \frac{\mathrm{NA}^2}{\lambda} \mathbf{f}^2 \right]^n. \tag{4}$$

Substituting Eq. (4) into Eq. (3), we can reformulate the defocused PSF $H(\mathbf{r}; h)$ as

$$H(\mathbf{r};h) = \sum_{n=0}^{N} h^n \varphi_n(\mathbf{r}), \tag{5}$$

$$\varphi_n(\mathbf{r}) = \mathtt{IFT}\left\{ \tilde{H}(\mathbf{f}) \frac{1}{n!} \left[j\pi \frac{\mathrm{NA}^2}{\lambda} \mathbf{f}^2 \right]^n \right\}. \tag{6}$$

It is noted that the process variable defocus h and the coordinate $\mathbf{r}$ in defocused PSF $H(\mathbf{r}; h)$ are separated.

Subsequently, putting Eq. (5) into Eq. (2), we obtain a variable-separated DIR function with the truncation order N as

$$D(\mathbf{r}_1, \mathbf{r}_2; h) = \sum_{n=0}^{N} h^n D_n(\mathbf{r}_1, \mathbf{r}_2), \tag{7}$$

Downloaded From: http://nanolithography.spiedigitallibrary.org/ on 04/11/2014 Terms of Use: http://spiedl.org/terms

$$D_n(\mathbf{r}_1,\mathbf{r}_2)=J(\mathbf{r}_1-\mathbf{r}_2)\left\{\sum_{i=0}^{n}\varphi_i(\mathbf{r}_1)\varphi_{n-i}^{\dagger}(\mathbf{r}_2)\right\}. \tag{8}$$

It is noted that $D_n(\mathbf{r}_1, \mathbf{r}_2)$ is Hermitian and can be singular-value decomposed as

$$D_n(\mathbf{r}_1,\mathbf{r}_2)=\sum_{k=1}^{K}\mu_{nk}\phi_{nk}(\mathbf{r}_1)\phi_{nk}^{\dagger}(\mathbf{r}_2), \tag{9}$$

where $\phi_{nk}(\mathbf{r})$ is the k-th kernels with K kernels in total, and μ_{nk} is its corresponding eigenvalue. Substituting Eq. (9) into Eq. (7) and then into Eq. (1), the defocused optical image $I(\mathbf{r}; h)$ is rephrased as

$$I(\mathbf{r};h)=\sum_{n=0}^{N}h^n I_n(\mathbf{r}), \tag{10}$$

$$I_n(\mathbf{r})=\sum_{k=1}^{K}\mu_{nk}\left|\phi_{nk}(\mathbf{r})\otimes M(\mathbf{r})\right|^2. \tag{11}$$

Here, $\otimes$ denotes the 2D convolution. It is noted that the basis image $I_n(\mathbf{r})$ is independent of defocus which thus may be calculated and stored in advance. So the defocused optical images can be calculated efficiently and accurately by summing pre-computed and stored partial images $I_n(\mathbf{r})$ weighted by the coefficients h^n. The significance of Eq. (10) lies in that the fixed mask-kernel convolutions are fully separated from the process variable, defocus, and can be pre-computed, so that optical images under a large range of defocus can be quickly calculated. This is the fundamental rationale behind the CVS method.

The defocused optical image $I(\mathbf{r}; h)$ goes through the resist development to form the printed image on the wafer. The resist effect can be approximated by a constant threshold resist model using the following Sigmoid function,

$$\mathrm{sig}\left[I(\mathbf{r};h);t\right]=\frac{1}{1+\exp\{-a[I(\mathbf{r};h)-t]\}}. \tag{12}$$

where a is the steepness of the Sigmoid function and t is the threshold level of the resist. Specifically, exposure dose variation can be accounted for by varying the threshold t.

In this work, we use $Z(\mathbf{r})$ to denote the output pattern on the wafer of the input mask $M(\mathbf{r})$ under the defocus h and dose variation t. Combining Eqs. (10) and (12), we can formulate the lithography imaging equation as

$$Z(\mathbf{r};h,t)=\mathrm{sig}\left[I(\mathbf{r};h);t\right]=\mathrm{sig}\left[\sum_{n=0}^{N}h^n I_n(\mathbf{r});t\right]. \tag{13}$$

2.2 Formulation of robust inverse lithography

We formulate the robust inverse lithography problem as

$$M^*=\arg\min_{M}\left[G(M)+\kappa R(M)\right], \tag{14}$$

$$G(M)=\sum_{p}^{P}\sum_{q}^{Q}\left\{\alpha(h_p)\beta(t_q)\left[\frac{\delta_x\cdot\delta_y}{L}\cdot\left\|Z(\mathbf{r};h_p,t_q)-Z^*(\mathbf{r})\right\|_2^2\right]\right\}. \tag{15}$$

Here, $R(M)$ is regularization term with the corresponding weight κ to promote mask manufacturability, $G(M)$ is called statistical edge distance error (EDE) [11, 12] to evaluate the difference between the output pattern of input mask $M(\mathbf{r})$ and the desired pattern $Z^*(\mathbf{r})$ on the wafer, δ_x and δ_y are the lengths of the discretized mask grid along the x and y directions, respectively, L is the perimeter of the desired pattern contour, $\alpha(\cdot)$ is the density of a prescribed distribution of defocus, $\beta(\cdot)$ is the density of a prescribed distribution of exposure dose, $Z(\mathbf{r}; h_p, t_q)$ represents the output pattern of the defocused image $I(\mathbf{r}; h_p)$ on the wafer under the exposure dose level t_q, and $\|\cdot\|_2$ is the L_2 norm. Equation (14) may be solved by an optimization algorithm [8], in which the forward lithography imaging simulation is iterated many times and each iteration requires calculating a total of P defocused images.

Downloaded From: http://nanolithography.spiedigitallibrary.org/ on 04/11/2014 Terms of Use: http://spiedl.org/terms

3. SIMULATIONS

Simulations were performed on a partially coherent imaging system with a quasar source illumination (σ_{out}/σ_{in}/degree = 0.9/0.6/45º). The wavelength in the simulations was set at 193 nm, and the numerical aperture (NA) was 1.35. The resist effect was approximated by a Sigmoid function with a = 100 and t = 0.4. All the simulations were carried out with in-house Matlab codes on a HPZ820 Workstation.

3.1 Computational complexity analysis of convolution-variation separation method

From the definition of robust inverse lithography problem in Sec. 2.2, numerous optical images under different defocus are required to be calculated and repeated in each iteration. In conventional approaches, to calculate P discrete sampling points of defocus, they need to generate and use P sets of process models. Let T denote the computational complexity for simulating one sampling point of defocus, and let $T(P)$ be the total computational complexity for simulating P sampling points of defocus; then the following formula holds true for all conventional approaches:

$$T(P) = T \times P. \tag{16}$$

In the presented CVS method, let T_0 denote the computational complexity of calculating all basis images $I_n(\mathbf{r})$ in Eq. (11), and let δT denote the extra complexity for summing up the series in Eq. (10). It is usually the case that $\delta T \ll T_0$ and $T_0 \approx T \times (N + 1)$, where N is the truncation order of Eqs. (5) and (7). Therefore, the computational complexity for simulating one defocus sampling point is $T_{CVS}(1) = T_0 + \delta T$, whereas the cost for simulating P sampling points of defocus would be

$$T_{CVS}(P) = T_0 + \delta T \times P. \tag{17}$$

As demonstrated in Fig. 1, the advantage of using CVS method become apparent as the defocus number $P > (N + 1)$, and gets larger.

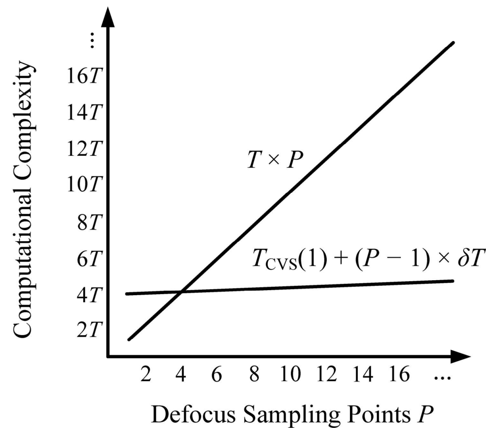

Figure 1. Computational complexity of the conventional approaches and the CVS method for simulating P defocus sampling points. T denotes the computational complexity of the conventional approaches for simulating one defocus sampling point. Here, we set the truncation order $N = 3$.

3.2 Results of robust inverse lithography

Figure 2 shows a desired output pattern on the wafer with CD of 32 nm. The pattern has a size of 401×401 pixels with a pixel size of 2 nm. The synthesized input mask patterns under different defocus and exposure dose distributions are shown in Fig. 3. As expected, different distributions result in different mask patterns. Moreover, it is particularly interesting to observe that the sub-resolution assist features (SRAFs) in Figs. 3(a) and 3(e) are dramatically different. That means different SRAFs patterns correspond to different process distributions.

Figures 3(d) and 3(h) depict the exposure-defocus (E-D) trees of the synthesized mask patterns by setting the EDE [11, 12]

Downloaded From: http://nanolithography.spiedigitallibrary.org/ on 04/11/2014 Terms of Use: http://spiedl.org/terms

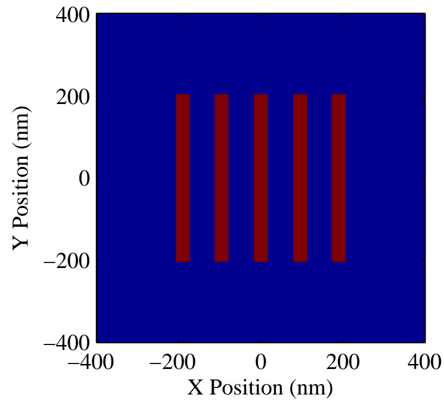

Figure 2. Desired pattern on the wafer.

to within ±10% of the CD target. To clearly show the process distribution, we draw the E-D window along with its probability distribution. It demonstrates that the proposed robust inverse lithography is sensitive to the difference of the process distribution, and it has the capacity of synthesizing a mask pattern to match the distribution.

4. CONCLUSIONS

In this work, we formulate the robust inverse lithography in a statistical manner, and employ a CVS method to calculate numerous defocused optical images. Benefiting greatly from the CVS method, we can take numerous defocus sampling points to exactly model its real distribution without proportionally increasing the computational complexity. Compared to conventional approaches, the superior scalability of the CVS method is apparent when the number of defocus gets larger. In addition, we observe that different process distributions result in mask patterns with dramatically different SRAFs in robust inverse lithography. Therefore, it has practical significance to consider the real process distribution in

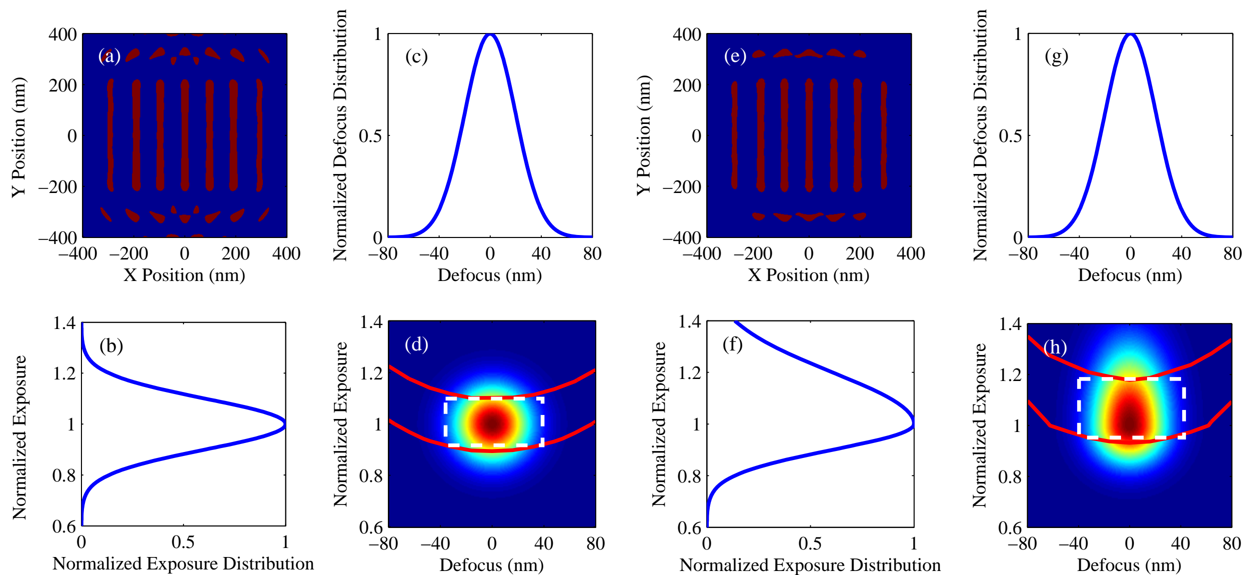

Figure 3. (a) The synthesized mask pattern under the exposure distribution (b) and defocus distribution (c), (d) is its E-D window. (e) The synthesized mask pattern under the exposure distribution (f) and defocus distribution (g), (h) is its E-D window.

Downloaded From: http://nanolithography.spiedigitallibrary.org/ on 04/11/2014 Terms of Use: http://spiedl.org/terms

robust inverse lithography to raise yield.

ACKNOWLEDGMENT

This work was funded by the National Natural Science Foundation of China (Grant No. 91023032, 51005091, 51121002), the Specialized Research Fund for the Doctoral Program of Higher Education of China (Grant No. 20120142110019), the National Science and Technology Major Project of China (Grant No. 2012ZX02701001), and the National Instrument Development Specific Project of China (Grant No. 2011YQ160002).

REFERENCES

[1] A. K. Wong, *Resolution Enhancement Techniques in Optical Lithography* (SPIE Press, 2001).
[2] D. O. S. Melville, A. E. Rosenbluth, A. Waechter, M. Millstone, J. Tirapu-Azpiroz, K. Tian, K. Lai, T. Inoue, M. Sakamoto, K. Adam, and A. Tritchkov, "Computational lithography: Exhausting the resolution limits of 193-nm projection lithography systems," J. Vac. Sci. Technol. B **29**, 06FH04 (2011).
[3] N. Jia and E. Y. Lam, "Machine learning for inverse lithography: using stochastic gradient descent for robust photomask synthesis," J. Opt. **12**, 045601 (2010).
[4] Y. Shen, N. Jia, N. Wong, and E. Y. Lam, "Robust level-set-based inverse lithography," Opt. Express **19**, 5511-5521 (2011).
[5] B. E. A. Saleh, "Optical bilinear transformations: General properties", Opt. Acta **26**, 777-799 (1979).
[6] H. H. Hopkins, "On the diffraction theory of optical images," Proc. R. Soc. A **217**, 408–432 (1953).
[7] N. B. Cobb, "Fast optical and process proximity correction algorithms for integrated circuit manufacturing," Ph.D. Dissertation (University of California at Berkeley, 1998).
[8] P. Gong, S. Y. Liu, W. Lv, and X. J. Zhou, "Fast aerial image simulations for partially coherent systems by transmission cross coefficient decomposition with analytical kernels," J. Vac. Sci. Technol. B **30**, 06FG03 (2012).
[9] W. Lv, S. Y. Liu, Q. Xia, X. F. Wu, Y. Shen, and E. Y. Lam, "Level-set-based inverse lithography for mask synthesis using the conjugate gradient and an optimal time step," J. Vac. Sci. Technol. B **31**, 041605 (2013).
[10] S. Y. Liu, X. J. Zhou, W. Lv, S. Xu, and H. Q. Wei, "Convolution-variation separation method for efficient modeling of optical lithography," Opt. Letter **38**, 2168-2170 (2013).
[11] W. Lv, Q. Xia, and S. Y. Liu, "Pixel-based inverse lithography using a mask filtering technique," Proc. SPIE **8683**, 868325 (2013).
[12] W. Lv, Q. Xia, and S. Y. Liu, "Mask-filtering-based inverse lithography," J. Micro/Nanolith. MEMS MOEMS **12**, 043003 (2013).

Downloaded From: http://nanolithography.spiedigitallibrary.org/ on 04/11/2014 Terms of Use: http://spiedl.org/terms